presented at the "Third International Symposium on Cavitation Noise and Erosion in Fluid System" of the ASME Winter Annual Meeting, December 1989, San Francisco, California.

# SHOCK PRESSURE GENERATED BY CAVITATION VORTEX COLLAPSE

F. Avellan, Senior Research Scientist and M. Farhat, Research Assistant
IMHEF
EPFL- Swiss Federal Institute of Technology of Lausanne,
Lausanne, Switzerland

## ABSTRACT

Most of the severe erosion of hydraulic machines are found to be associated with the collapse of transient cavitation vortices downstream of a leading edge cavity. The dynamics of such a type of cavitation is studied in a Cavitation Vortex Generator (CVG). By producing the cyclic growth and collapse of single cavitation vortex, this device provides a way to investigate the mechanisms involved in the final stage of the cavity collapse.Very high speed visualization, at a rate of 500 '000 frames per second, reveals a strong spherical shock-wave emitted at the time of the cavitation vortex collapse. Thus, the image processing of these high-speed photography allows us to measure the cavity wall velocity and the shock wave celerity in order to estimate the shock pressure. These estimations lead to mean values of 900 MPa and extreme values as high as 2'200 MPa. Moreover a new optical arrangement can make the shock-waves visible both in the fluid and in a perspex specimen fitted in the the test section.

## NOMENCLATURE

| | | | |
|---|---|---|---|
| $a_0$ | = | Speed of sound in water | [m·s$^{-1}$] |
| $c$ | = | Shock wave celerity | [m·s$^{-1}$] |
| $B$ | = | Constant of Tait's equation | [Pa] |
| $l_c$ | = | Cavity length | [m] |
| $p$ | = | Static pressure | [Pa] |
| $p_{ref}$ | = | Reference pressure (downstream vessel) | [Pa] |
| $p_v$ | = | Vapor pressure | [Pa] |
| $Q$ | = | Flow rate | [m$^3$·s$^{-1}$] |
| $R$ | = | Inlet pipe radius | [m] |
| $R_{in}$ | = | Inlet chamber radius | [m] |
| $R_{out}$ | = | Outlet pipe radius | [m] |
| $R_s$ | = | Spherical shock wave radius | [m] |
| $U$ | $= \frac{Q}{\pi R^2}$ | Mean axial velocity in the inlet pipe | [m·s$^{-1}$] |
| $U_{out}$ | $= \frac{Q}{\pi R_{out}^2}$ | Mean velocity in the outlet pipe | [m·s$^{-1}$] |
| $V$ | = | Mean velocity of the cavity wall | [m·s$^{-1}$] |
| $\delta t$ | = | Time interval | [s] |
| $\Delta p$ | = | Shock pressure | [Pa] |
| $\Omega$ | = | Flow vorticity | [rad·s$^{-1}$] |
| $\rho$ | = | Water density | [kg·m$^{-3}$] |
| $\rho_0$ | = | Water density for standard conditions | [kg·m$^{-3}$] |
| $C_p$ | $= \frac{p - p_{ref}}{\frac{1}{2}\rho U^2}$ | Pressure coefficient at the center axis | [-] |
| $C_{pwall}$ | = | Wall pressure coefficient | [-] |
| $M$ | $= \frac{c}{a_0}$ | Mach number | [-] |
| $\sigma$ | $= \frac{p_{ref} - p_v}{\frac{1}{2}\rho U^2}$ | Cavitation number | [-] |

## INTRODUCTION

The use of specific facilities such as the IMHEF universal hydraulic machine test loop [1] and the IMHEF high-speed cavitation tunnel [2] allows us to study the type of cavitation associated with erosion of hydraulic machines. By comparisons between cavitation tests on models and damage observations on prototype of hydraulic machines we could identified, the erosive cavities involved in severe erosion of both types of hydraulic machines, pumps and turbines, as transient cavitation vortices which collapse in the closure region of a leading edge main cavity, [3]. Therefore the generation process of these transient cavities and their interaction with the mean flow in the case of the development of a leading edge cavity at high Reynolds number have been studied [4]. In order to investigate the dynamics of such cavities, we decided to use a special vortex cavitation generator. The description of this cavitation vortex generator (CVG) and the main physical mechanisms leading to the material damage were given in [5]. By producing a cyclic growth and collapse of a single cavitation vortex we can study the cavity dynamics in the test section of the CVG and the related damage of different test specimens. A systematic comparison [6] of the various cavitation erosion situations has already been carried out to see whether the CVG was able to produce the same cavitation erosion compared to the damages observed in hydraulic machinery.

The aim of this paper is to describe the dynamics of the final stage of the cavitation vortex collapse observed in the CVG in order to explain the hydrodynamic process by which material damages are caused. First, we describe briefly the CVG and the hydraulic operation of that device. The experimental set-up, involving the high-

speed Cranz-Schardin camera and the pressure instrumentation, is then presented. Finally the image processing of high-speed photography is carried out in order to measure the cavity wall velocity and the shock wave celerity. By using the Tait's equation of state for water we can compute the Mach number and the shock overpressure related to the bulk pressure evolution in the CVG test section and the shock wave propagation in a perspex specimen fitted at the end of the test section.

## THE CAVITATION VORTEX GENERATOR

### Principle of operation

The cavitation vortex generator is a hydraulic closed loop consisting of a test section where erosion tests and visualization can be carried out, a rotating valve, a set of vessels and a circulating pump, see Figure 1. The test section is made of a cylindrical chamber with 40 mm inner radius, $R_{in}$, and 20 mm width. The flow incomes into the cylindrical chamber through a tangential inlet of 5 mm radius, $R_{in}$. A 40 mm long truncated volume with a circular to a rectangular cross-section change, and a circular outlet of 12 mm radius, $R_{out}$, are located on each side of the inlet chamber on the same axis, see Figure 2. The rotating valve is made of a shutter fixed on the periphery of a disk driven by a DC motor. The valve velocity can be varied in the range of 0 to 1000 rpm. The multi-stage centrifugal pump is connected to the CVG circuit through two vessels with a volume of 60 l and provides a flow rate of up to 3 $m^3$/hour corresponding to a 9.5 bar total pressure. The flow rate can be adjusted by changing the pump speed. A heat-exchanger is installed at the pump outlet to keep the CVG water temperature constant. All the tests were done at 19°C.

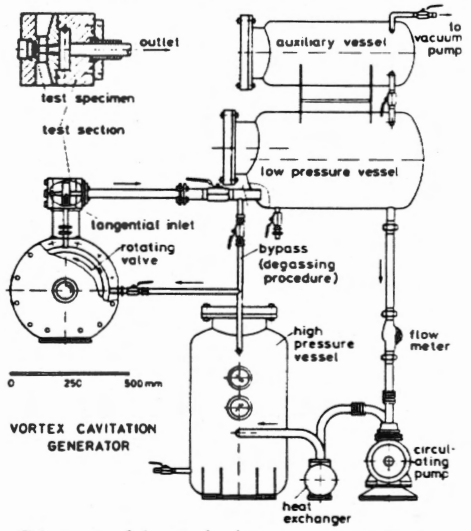


Fig. 1 Diagram of the cavitation vortex generator

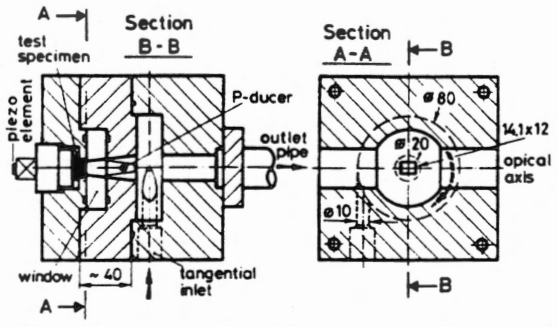


Fig. 2 Side and top views of the test section of the CVG *(all the dimensions are in mm).*

The principle of the CVG is to produce, at each revolution of the rotating valve, a series of expansion-compression waves in order to promote cyclic growth and collapse of cavities in a vortex flow field. During the open valve position, which is 96% of one valve-revolution, the tangential inlet flow induces a rotational motion in both the truncated volume of the test section and the outlet pipe. In the outlet pipe, an axial motion is combined with a vortex flow centered on the test section axis. The vorticity line extends downstream to the vessel and upstream to an axisymmetrical stagnation point at the end of the truncated volume where the test specimen is fitted. In the center part of the flow, the viscosity effect leads to a free vortex flow field with a solid body rotation core.

At the flow cut-off, the resulting water-hammer generates an expansion wave in the test section. Water-hammer transient calculations show that flow vaporization occurs already at the valve during the final stage of the flow cut-off, though the valve is not yet completely closed. However, depending on the wave transit times, the pressure in the test section is decreasing gradually up to the vaporization of the vortex core. As long as the valve is closed, the cavitation extends into the central part of the test section. When the valve opens, the overpressure at the valve forces the cavity to collapse. The operation remains efficient as long as the CVG circuit water is deaerated. The presence of dissolved gases leads to the growth of a steady gaseous cavity in the test section, even during the open position of the valve, and then prevents the CVG to operate efficiently. However, before each test, and at least every day, a special degassing procedure is carried out with a vacuum pump. The gas content of the water is monitored with an oxygen probe and kept lower than 0.2 ppm.

### Hydraulic operation

Cavitation vortices are directly controlled in the CVG by three operating parameters. On one hand the pump flow rate Q and the back-pressure $p_{ref}$ in the downstream vessel impose the overpressure at the valve opening and the steady pressure distribution in both the test section and the outlet pipe. On the other hand the valve rotation speed which obviously gives the duration of the closed valve position, limits the size of the cavity extension in the test section.

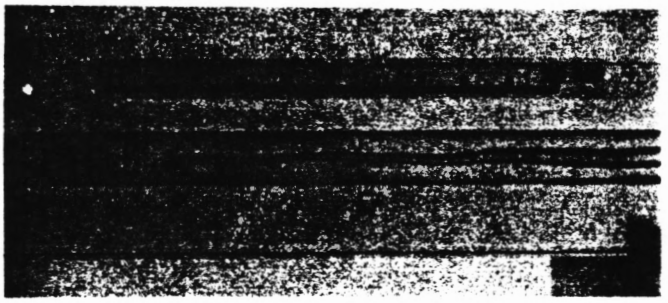

Fig. 3 Vaporization of the vortex core in the outlet pipe. Steady conditions, Q = 0.62 l/s, $\sigma$ = 0.31 *(Flow from right to left).*

In order to study the influence of back-pressure and flow rate for steady conditions, static pressures have been measured in the center of the end of the test section, and at the wall of two sections of the outlet pipe, see Figure 5. If the static pressure in the test section center is obviously given directly through the pressure tap on the test specimen wall, we have to extrapolate the center pressure in the outlet pipe from the wall pressure. Thus by varying $p_{ref}$ it is possible to quote the different pressure values corresponding to the onset of core vaporization in the outlet pipe, as it can be seen in the photography of Figure 3. Therefore according to the normalization of the CVG operating parameters given in the nomenclature the pressure difference between the wall and the center of the pipe can be expressed as the following non-dimensional equation :

$$Cp_{wall} - Cp = Cp_{wall} + \sigma \text{ at cavitation inception}$$

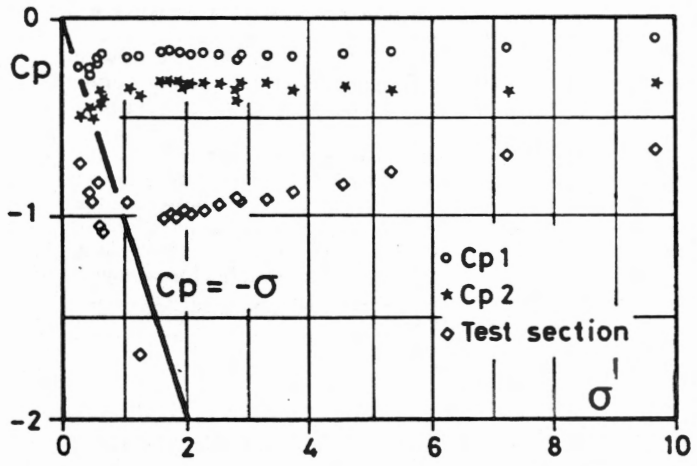


Fig. 4 Pressure coefficient evolution versus σ along the axis at the test section and both end of the outlet pipe. *Data under the solid line Cp = -σ correspond to vapor in the pressure line .*

The pressure coefficient curves against the cavitation number σ are given Figure 4 and correspond to the three above mentioned locations along the mean axis of the swirling motion. The line Cp = σ allows us to predict the core vaporization onset. We can observe that the lowest pressure takes place in the test section and cavitation inception occurs for a σ value of 1.2. However the CVG operation of interest corresponds to cavitation free steady condition.

Moreover if we assume a solid body rotation in the inlet chamber of the test section of radius $R_{in}$, an estimation of the flow vorticity Ω is given by the ratio

$$\frac{\Omega R_{in}}{U} = 1 \qquad [-]$$

Through the same assumption, this value can be also estimated in the outlet pipe and related to the mean axial velocity $U_{out}$ in the outlet pipe. At both end of the outlet pipe, we obtain the following values for the ratio $\Omega R_{out}/U_{out}$ .

| Q [m³/s] | Section #1 [-] | Section #2 [-] |
|---|---|---|
| 0.615 $10^{-3}$ | 1.44 | 0.37 |
| 0.741 $10^{-3}$ | 1.90 | 0.90 |

These values fairly show the vorticity decay of the flow in the outlet pipe and the influence of the Reynolds number.

## INSTRUMENTATION

### Pressure instrumentation.

To record pressure time history with respect to cavitation development in the test section and the outlet pipe, three pressure transducers are flush mounted at the same location as the pressure taps, at the wall of the test section, on the center axis and at both sides of the outlet pipe, see Figure 5. Three 601-A Kistler model quartz pressure transducers are used. These piezoelectric transducers have a 1 μs rise time, a 400 kHz eigen frequency and a 0 to 200 bar pressure range. Charge signal is amplified and voltage-converted through a TA 3/D Vibrometer charge-amplifier with a 300 kHz band pass limit. All the signal outputs are simultaneously sampled and stored on a transient recorder at 1 MHz sampling rate.

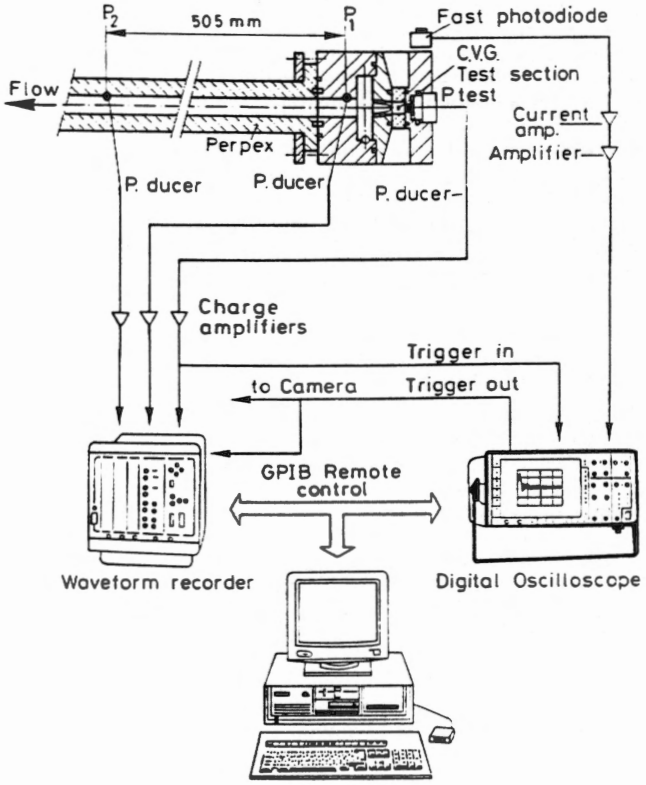


Fig. 5 Transducer locations and data sampling system

### High-speed camera

A high-speed shadowgraph system is used to visualize the transient phenomena involved in the CVG test section. This is achieved with a Cranz-Schardin camera, which is an improved system based on an Institute of Saint Louis (West Germany) design [7]. This camera consists of a set of 16 spark generators used as short-duration light sources giving a mean exposure time of 300 ns, and 16 corresponding achromat objectives which provide 16 frames on the same 4" x 5" photographic plate placed at the back plane of the camera as shown in Figure 6. The discharges are controlled by an electronic time-unit which provides an adjustable spark rate of 1 kHz to 10 MHz with a constant time resolution of 50 ns between each trigger pulse. Nevertheless a fast photodiode of 1 ns of rise time and 350 MHz of band width is used in order to check the true spark period with respect to the pressure signals. As a part of the test section itself, a highoptical quality glass window is installed just in front of the test specimen. The window is made of bonded glass blocks of ground parallel faces and is coated on the external faces to overcome light reflection.

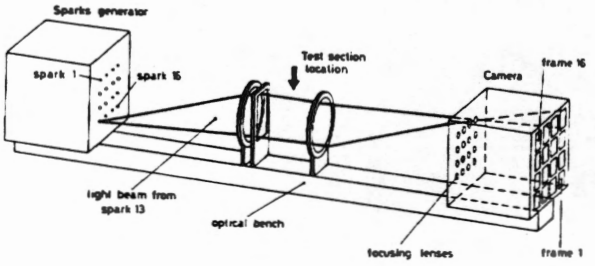


Fig. 6 Optical arrangement of the high-speed Cranz-Schardin camera

### Camera triggering

Camera triggering is the main difficulty of this experimental work. Owing to our aim to record transient phenomena produced by the cavity collapse, we need frame periods of less than 3 µs. However only 16 frames are available and therefore the trigger signal requires an accuracy and repeatability of less than 10 µs. Multiple trials have been carried out. For instance, the trigger signal given by the rotating valve closure was found to be uncertain, jitter of about 2 ms, since the time lag between the trigger and the collapse was too long (≈ 20 ms). The pressure signal from the transducer mounted in the specimen was found to be the best way to trigger both the camera and the transient recorder as well. This was done by picking up the internal trigger of a digital oscilloscope at 50 MHz sampling rate which provides the capability of adjusting the level and delaying the trigger signal itself.

## CAVITY VISUALIZATION

### Cavity life cycle

Simultaneous recordings of pressure signals combined with photography sequence allow us to investigate the explosive growth and the collapse of cavitation vortex in the CVG section. As it is shown in Figure 7, the pressure signal in the test section indicates a static pressure decrease down to the vapor static pressure, due to the water hammer resulting at the flow cut-off about 7 ms after the start of the valve closing. The corresponding Cranz Schardin photography sequence of the explosive growth of a cavitation vortex is given Figure 9. Time delay is set at 7 ms from the start of the valve closing and the spark period is 200 µs. First the liquid is ruptured in the form of individual cavities along the vortex axis. When all these cavities are gathered to fill the vortex core the cavitation extends radially to the whole region of the pressure drop. The mean radial velocity of the wall cavity motion is about 1.7 m/s.

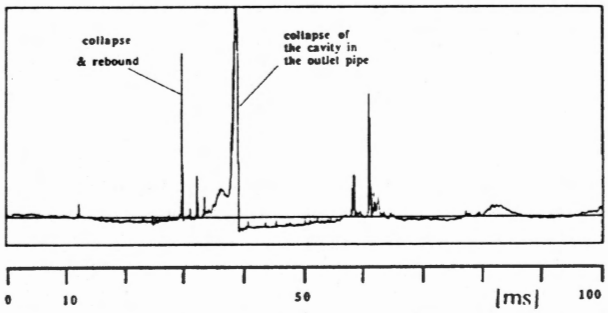


Fig. 7 Pressure signal in the test section corresponding to frame sequence of figure 8

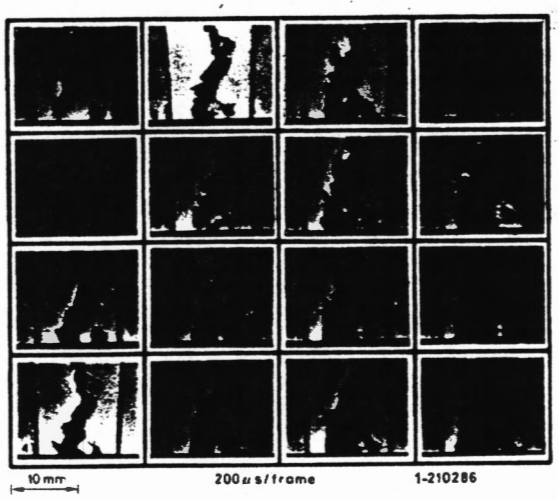


Fig. 8. Explosive growth of the cavitation vortex. Spark period : 200 µs, Q = 0.83 l/s, σ = 0.89.

The outward motion of the cavitation vortex is inverted when the incoming flow from the valve arrives in the test section. It takes 6 ms for the cavitation to disappear from the test section. Thereafter a high pressure peak is detected by the transducer leading to the 1st peak of the signal of Figure 7. This corresponds to the cavitation vortex collapse in the test section which is immediately followed by a cavity rebound and shock wave generation well visible in the sequences of Figures 9,10 and 11. A second pressure peak, detected by the pressure transducers is due to the cavity collapse in the outlet pipe. Hence, successive pressure wave series occur between the downstream vessel and the test section leading to successive collapse and cavity rebound of the vortex core. This phenomenon, which is driven by water mass oscillation, is rapidly damped, but the strongest collapse, which causes the material damage of the test specimen, is the first occurring after the valve opening.

### Cavitation vortex collapse

Due to short time constants involved, pressure transducers are unable to track the cavitation vortex collapse dynamics. Cranz-Schardin visualizations allow us to follow cavity wall motion and resulting pressure waves as long as the sequence of the 16 frames fall in the collapse time-history of interest. The frame sequences presented in Figure 9, 10 and 11 correspond to the final stage of the cavitation vortex collapse. Both of them are taken with a frame period of 1µs, the rotating valve speed of 200 RPM. In the case of Figure 9 and 10 the 0.89 cavitation number is the same and the flow rate is respectively 0.68 $10^3$ $m^3/s$ and 0.8 $10^3$ $m^3/s$. Sequence of Figure 11 corresponds to a lower flow rate of .53 $10^3$ $m^3/s$ and a 2.4 σ value. On Figure 9 and Figure 11 frame sequences the cavity collapses between the 2nd and the 3rd frame. The spherical shock wave, which results from the cavity rebound and its reflections are well visible in the following frames. In the case of Figure 10 the cavity collapse takes place between the 4th and the 5th frame. On the three figures the corresponding signal of the pressure transducer fitted at the end of the test section is reported. In all the cases the transducer is over saturated, since it is rated at 20 MPa. The high energy sparks of the flashes trig a 400 kHz resonance of the transducer which is visible on the signal and allows to monitor the flash time history. A time delay of about 4 µs can be observed between collapse of the cavity and rise of the signal corresponding to the rise time of the charge amplifier. Up to 23 successful shots like those given in the last figures have been carried out by varying the flow rate Q and the cavitation number σ. The number of cases corresponding to the operating conditions are given in the following table.

| σ \ Q | 0.54 l/s | 0.68 l/s | 0.80 l/s |
|---|---|---|---|
| 1.5 | 4 | 1 | -- |
| 1.9 | 5 | 5 | 6 |
| 2.4 | 2 | -- | -- |

## SHOCK PRESSURE

Visualizations of cavity wall motion and shock wave provide a way to calculate the overpressure through the shock wave. Thus, by digitizing the photography of each sequence, we can follow the actual wall motion of the cavity by fitting an ellipse through the cavity contour. This provides an estimation of major and minor axis lengths and center coordinates of the cavity. The same process is achieved with spherical shock wave radiated after the collapse giving us radius and center coordinates for every spark period. In all the cases, center of the spherical shock waves corresponds to that of the cavity. All these data can be derived in order to compute the mean cavity wall velocity V and the shock wave celerity c. It can be observed that, since the second frame after the collapse occurs, the shock wave celerity c is decreasing up to to the speed of sound $a_0$ = 1500 m/s.

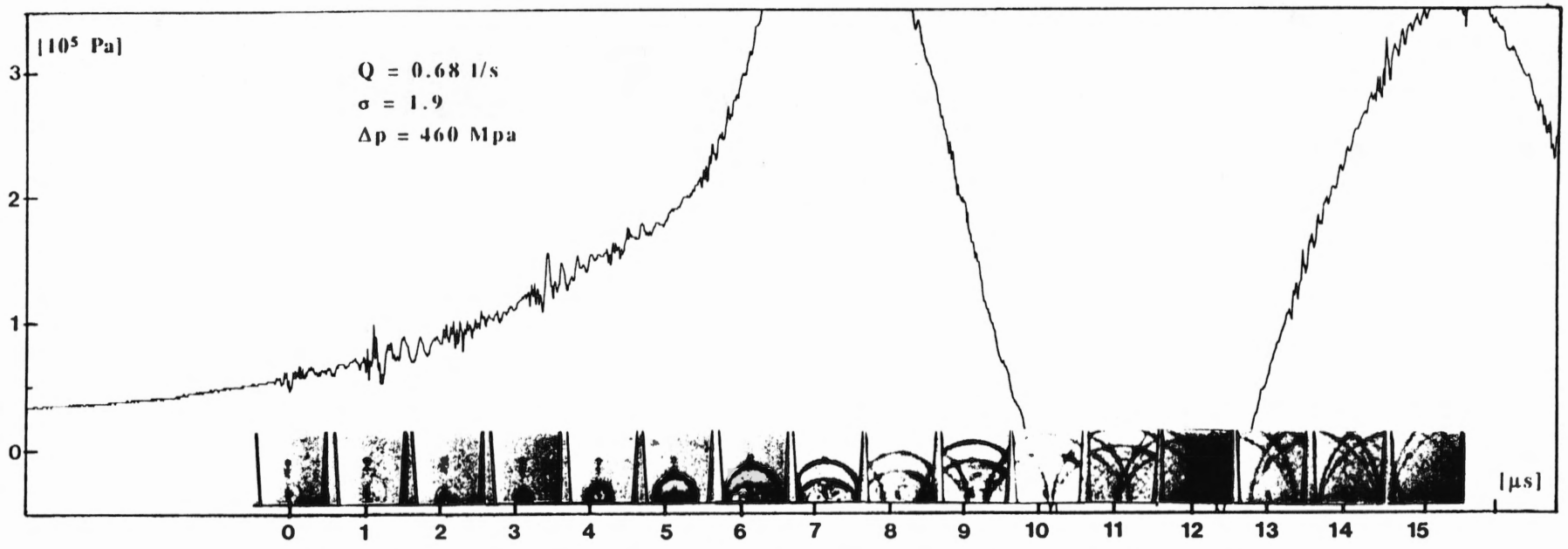


Fig. 9 Test section pressure signal and frame sequence of a cavity collapse: Q = 0.68 l/s, σ = 1.9, Δp = 460 Mpa

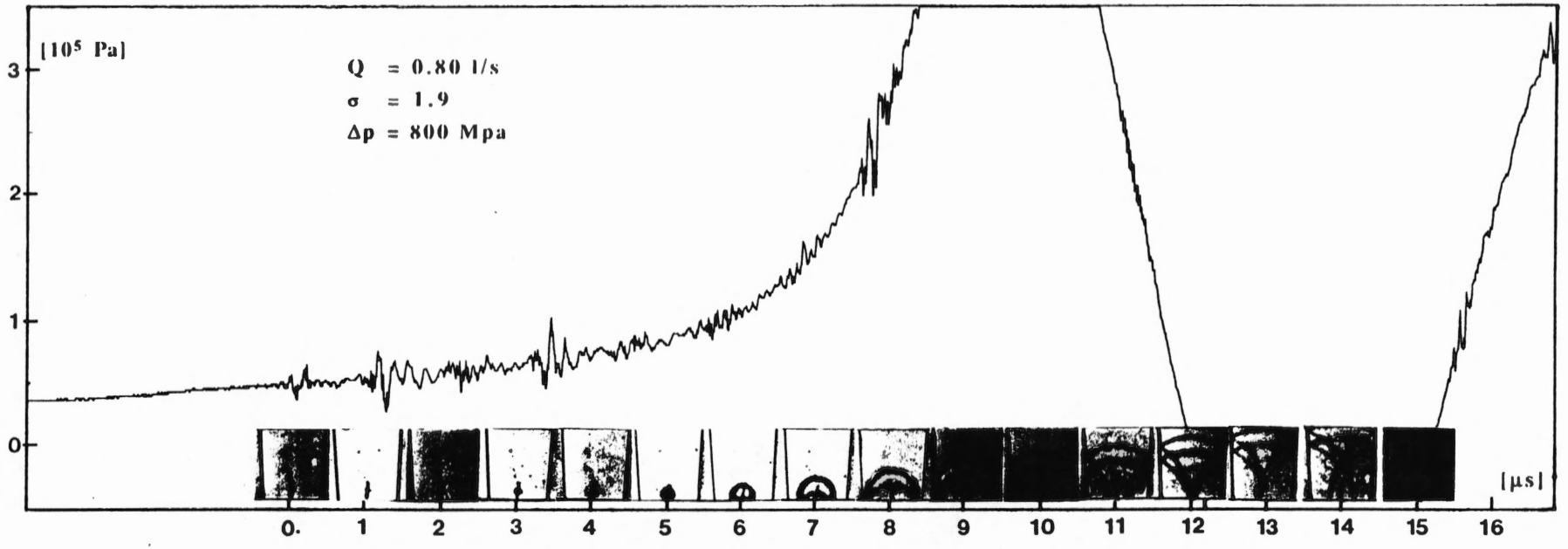


Fig. 10 Test section pressure signal and frame sequence of a cavity collapse: Q = 0.80 l/s, σ = 1.9, Δp = 800 Mpa

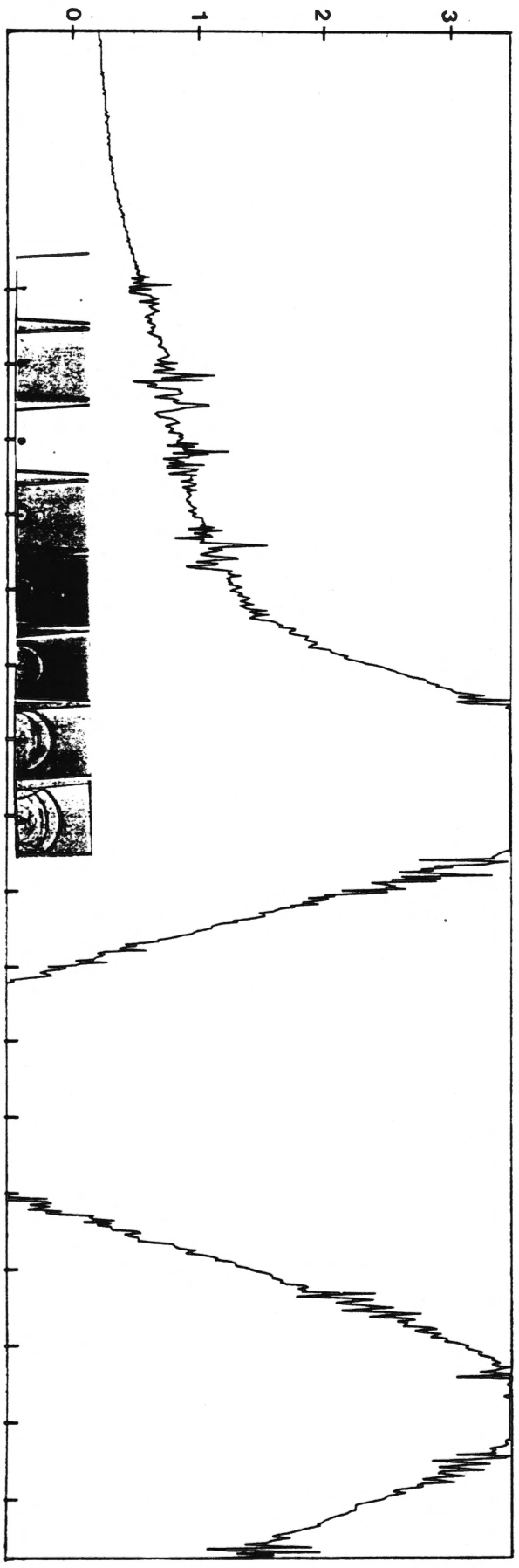

Fig. 11 Test section pressure signal and frame sequence of a cavity collapse: Q = 0.53 l/s, σ = 2.4, Δp = 420 Mpa

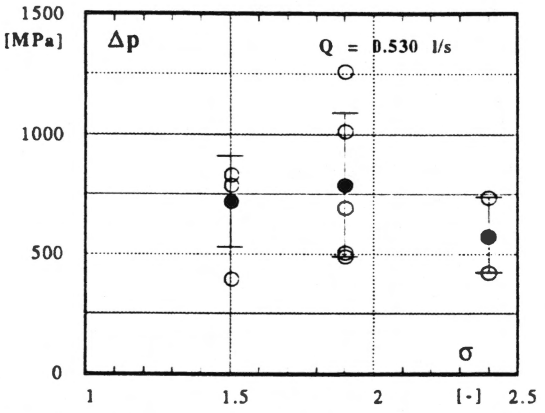


Fig. 12 Shock pressure obtained from the Cranz Schardin visualization

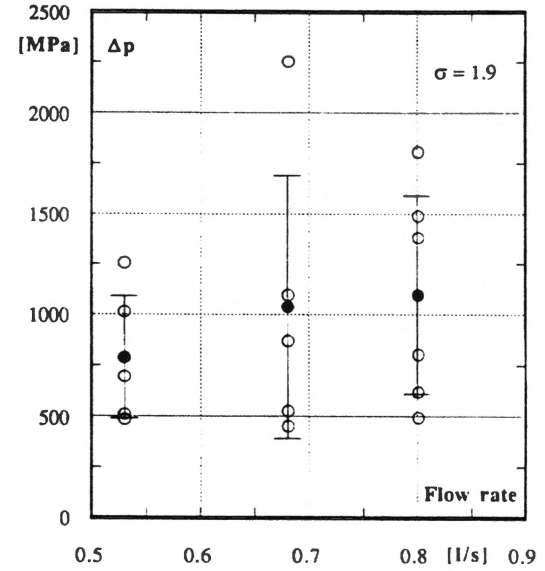


Fig. 13 Shock pressure obtained from the Cranz Schardin visualization

Moreover, if we assume that the time interval $\delta t$ between the collapse time and the instant corresponding to the next frame is known, we can approximate to the first order the cavity wall velocity V and the shock wave celerity c after the collapse by:

$$V = \frac{l_c}{\delta t} \quad \text{and} \quad c = \frac{R_s}{\delta t} \qquad [m \cdot s^{-1}]$$

where $l_c$ is the cavity half-length after the rebound and $R_s$ in the shock wave radius, these two values being taken from the first frame after the collapse.

The normal shock wave relation allows us to estimate from these data the shock wave overpressure $\Delta p$ by :

$$\Delta p = \rho_0 \, cV \qquad [Pa]$$

where $\rho_0$ is the density of water at ambient conditions.

However if the shock wave Mach number is known, it is then possible to calculate a new overpressure value according to the procedure given in [8].

Both the Tait's equation of state for water, given by :

$$\frac{\Delta p}{B} = (\rho/\rho_0)^7 - 1 \qquad [-]$$

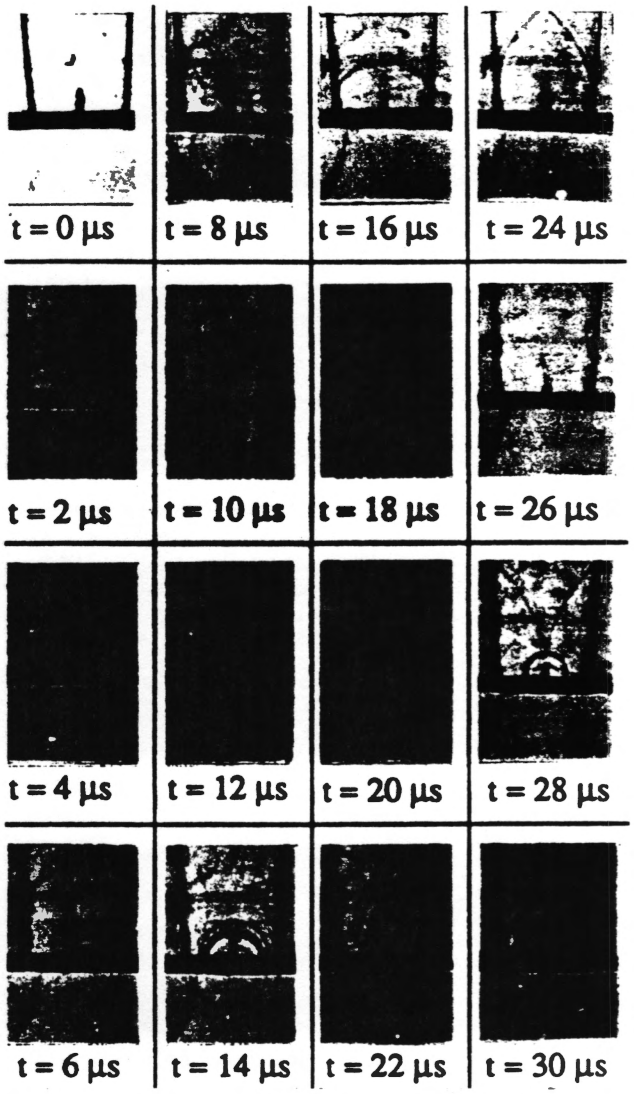


Fig. 12 Shock wave propagation both in water (top) and in the perspex test specimen (bottom). Q = 0.8 l/s, $\sigma$ = 1.9, $\Delta p$ = 460 MPa

and the equations of mass and momentum balance through the shock lead us to the following relation between Mach number M = c/a0 and density ratio $\rho/\rho_0$ :

$$(\rho/\rho_0)^8 - (1+7M^2)\,\rho/\rho_0 + 7M^2 = 0 \qquad [-]$$

The value of the B factor in the Tait's equation, corresponding to a 1500 m/s sound velocity $a_0$, is 321.4 MPa .

The last equation provides the density ratio $\rho/\rho_0$ which in turns gives us the $\Delta p$ value by the use of the Tait's equation. It is then possible to compare the two values of $\Delta p$ computed from the previous relations. Since these values are very sensitive to the time interval value $\delta t$, we do not assume any value, but we adjust the time interval $\delta t$ in order to obtain a same overpressure value by the two methods. The collapse overpressure for every frame sequence is calculated by following this iterative procedure.

The corresponding values are reported as open symbols in Figure 11 and 12 versus the cavitation number $\sigma$ and the flow rate Q respectively. Closed symbols represent mean values and are associated with error bars. These values do not show any well marked trend, even though they seems to slightly increase when increasing the flow rate as we could expect, see Figure 11. The average of the full set of these estimations leads to a mean value of 900 MPa, and extreme values as high as 2'200 MPa are found. It is worth noting that these values are higher than the tensile strength of most of the industrial alloys.

To assert that the mechanism of shock waves is responsible for the material erosion we have placed at the end of the test section a perspex block with ground parallel faces. This transparent specimen allows us to follow the shock wave inside the material corresponding to the cavity collapse. In the frame sequence of Figure 13 two collapses are captured both associated with a spherical shock wave radiation in the liquid and in the solid, no microjet impingement leading to high compressive waves is found. The first collapse occurs between 12 µs and 14 µs and pressure calculation leads to a value of 460 MPa. The second falls between 26 µs and 28 µs and the propagation of the spherical pressure wave in the solid can be seen on the last two frames.

## CONCLUSION

High-speed visualization of cavity collapse in the Cavitation Vortex Generator allows us to have an insight into the basic phenomenon which causes material erosion. The cavity rebound which follows the collapse promotes a spherical shock wave leading to very high pressure. Calculations of shock pressure for 23 different visualization sequences lead to a mean value of 900 MPa, and extreme values as high as 2'200 MPa, the lowest being 420 MPa. Moreover visualization of the stress wave propagation into a perspex test specimen confirm that material damage is caused by very high pressure shock wave.

## ACKNOWLEDGEMENT

The authors wish to acknowledge all their colleagues from the EPFL Cavitation Group.This research is financially supported by the Swiss Federal "Commission d'Encouragement à la Recherche Scientifique", The Swiss Energy producers association "Nationaler Energie Forschung Fonds", The Sulzer Brothers company and the Vevey Engineering Works company.

## REFERENCES

[1] Henry, P., "Hydraulic machine model acceptance tests", *Proceedings of an International Conference on Hydropower Plant*, Water Power '85, Las Vegas, 1985, vol 2, pp. 1258-1267.

[2] Avellan, F., Henry. P. & Ryhming, I. L., "A new high speed cavitation tunnel for cavitation studies in hydraulic machinery", *Proc. of International Symposium on Cavitation Research Facilities and Techniques, ASME Winter Annual Meeting*, Boston (USA), FED: Vol. 57, Dec 1987, pp 49-60.

[3] Avellan, F. , Dupont, Ph., "Cavitation erosion of the hydraulic machines: generation and dynamics of erosive cavities", *Proc. of the 14th IAHR Symposium*, 20-23 June, 1988, Trondheim (Norway), pp. 725 -738.

[4] Avellan, F., Dupont, Ph., Ryhming, I.L., "Generation mechanism and dynamics of cavitation vortices downstream of a fixed leading edge cavity", Proc. of 17th Symposium on Naval Hydrodynamics, The Hague (The Netherlands), Aug. 29 - Sept. 2, 1988, Sessions V, pp. 1 - 13.

[5] Avellan, F., Karimi, A., "Dynamics of vortex cavitation involved in the erosion of hydraulic machines", Proceedings of 7th Int. Conf. on Erosion by Liquid and Solid Impact, 6-10 Sept. 1987, Cambridge (UK),.pp. 25-1, 25-8.

[6] Karimi, A., Avellan F., "Comparison of erosion mechanisms in different types of cavitation", WEAR, vol. 113, n°3, Dec 1986, pp. 305, 322.

[7] Henchoz, A., *Proc. of Conference on High-speed Photography and Photonics*, August 1978, Tokyo.

[8] Ridah, S., "Shock wawes in water", *J. of Applied Physics*, July 1988, vol. 64 (1), pp 152-158